

# Detecting quantum phase transition by high-harmonic spectroscopy in strongly correlated systems

Can Shao,<sup>1,\*</sup> Hantao Lu,<sup>2</sup> Xiao Zhang,<sup>3</sup> Chao Yu,<sup>1</sup> Takami Tohyama,<sup>4</sup> and Ruifeng Lu<sup>1,†</sup>

<sup>1</sup>*Institute of Ultrafast Optical Physics, Department of Applied Physics,  
Nanjing University of Science and Technology, Nanjing 210094, China*

<sup>2</sup>*School of Physical Science and Technology & Key Laboratory for Magnetism and  
Magnetic Materials of the MoE, Lanzhou University, Lanzhou 730000, China*

<sup>3</sup>*Institute for Theoretical Solid State Physics, Leibniz IFW Dresden, Helmholtzstr. 20, 01069 Dresden, Germany*

<sup>4</sup>*Department of Applied Physics, Tokyo University of Science, Tokyo 125-8585, Japan*

By employing an unbiased numerical method, we investigate the ultrafast dynamics of the correlated systems in one and two dimensions. For the extended Hubbard model on a periodic chain, the high-harmonic generation (HHG) of system close to the quantum critical point (QCP) is more intense than HHG in the neighboring two gapped phases, i.e., charge-density-wave and spin-density-wave states, especially in low-frequencies. The reason can be attributed to that the system in QCP is more sensitive to the external field and there are more optical-allowed excited states available to furnish photon-absorbing channels for this nonlinear processes. This feature provides a possibility of detecting the quantum phase transition by means of high-harmonic spectroscopy. We also expect to generate stronger HHG by irradiating materials with parameter settings close to QCP. In addition, we find that the even- or odd-order components of HHG can be used to distinguish the topologically ordered phases from locally ordered ones in a two-dimensional interacting Haldane model.

*Introduction.*— Quantum phase transitions (QPTs) are of extensive interest in condensed matter physics [1, 2] because they happen at zero temperature where the thermal fluctuations vanish and the uncertainty effects in quantum physics are manifested. Systems driven by the quantum fluctuations can produce exotic states and excitations, such as unconventional superconductivity [3]. In a many-body system, phase transition accompanied with the onset of a local order parameter occurs as a result of competing interactions. Experimental detections of QPTs are straightforward, which include conductivity, susceptibility or total magnetization in some spin systems [4, 5]. However, not all order parameters can be measured by such macroscopic measurements and they are not suitable for closer investigations of the quantum critical point (QCP) [6]. Instead, the dynamical response functions such as the frequency-dependent optical conductivity provide an important route to investigate the quantum criticality [7–19]. Due to the destruction of quasiparticles and the corresponding abundance of incoherent excitations in the vicinity of the QCP, the systems are expected to be much more sensitive to external perturbations than in the center of a phase [20, 21], especially on short time scales. Thus, one can expect that nonequilibrium and nonlinear behaviors are relatively active in such systems, which may play a role as promising tools to detect QPT and QCP.

Strong-field-driven dynamics and high-harmonic generation (HHG) are perhaps the most representative examples of nonlinear and nonperturbative optical processes [22, 23], which are widely expected to generate the attosecond light sources and provide new ultrafast imaging methods [24, 25]. HHG has been initially studied in atomic and molecular gas systems, in which a char-

acteristic plateau with a cut-off energy is well explained by the three-step model [25–30]. Subsequently, HHG observed in ZnO crystal is interpreted by intraband Bloch oscillations [31], and the extended three-step model is proposed [32] and recognized in the community of solid HHG (see [33–36] and references therein). Most recently, the studies of HHG have also touched on the field of strongly correlated systems in one dimension (1D) [37–40].

In this Letter, we shed new light on the detection of QPT by means of the high-harmonic spectroscopy. We first study the ultrafast dynamics of the half-filled extended Hubbard model on the 1D chain, based on the exact diagonalization (ED) method. Due to the sensitivity of system close to QCP that separates two gapped phases, i.e., the spin-density wave (SDW) and charge-density-wave (CDW) states, an enhancement of the HHG intensity can be observed. Meanwhile, the HHG spectroscopy with only odd-order components has a good correspondence with the optical conductivity in equilibrium. This might provide a new insight to explain the HHG plateau and cut-off energy in correlated systems. In two-dimension (2D), with a topological phase transition from Chern insulator (CI) to the CDW phase in the interacting Haldane model, such enhancement of HHG close to the QCP is not observed. However, different from that only odd-order components of HHG appear in CDW phase, both odd and even harmonic orders exist in CI phase. This could also be utilized to detect the quantum phase transition.

*Models and observables.*— We consider two models to calculate the HHG: the spinful extended Hubbard model and the spinless Haldane model with nearest-neighbour interactions, both at half filling. The former is defined

on a periodic chain, which reads

$$\hat{H} = -t_1 \sum_{\langle i,j \rangle, \sigma} \left( \hat{c}_{i,\sigma}^\dagger \hat{c}_{j,\sigma} + \text{H.c.} \right) + U \sum_i \left( \hat{n}_{i,\uparrow} - \frac{1}{2} \right) \times \left( \hat{n}_{i,\downarrow} - \frac{1}{2} \right) + V \sum_{\langle i,j \rangle} (\hat{n}_i - 1)(\hat{n}_j - 1), \quad (1)$$

where  $\hat{c}_{i,\sigma}^\dagger$  ( $\hat{c}_{i,\sigma}$ ) creates (annihilates) an electron at site  $i$  with spin  $\sigma = \uparrow, \downarrow$ , and  $\hat{n}_i = \hat{n}_{i,\uparrow} + \hat{n}_{i,\downarrow}$  is the number operator of electrons;  $t_1$  is the hopping constant;  $U$  and  $V$  are the strengths of the on-site and nearest-neighbor (NN) Coulomb-interactions, respectively. The lattice size is set to be  $L = 10$ .

On the honeycomb lattice, we study the half-filled spinless Haldane model with repulsive NN interactions:

$$\hat{H} = -t_1 \sum_{\langle i,j \rangle} (\hat{c}_i^\dagger \hat{c}_j + \text{H.c.}) - t_2 \sum_{\langle\langle i,j \rangle\rangle} (e^{i\phi_{ij}} \hat{c}_i^\dagger \hat{c}_j + \text{H.c.}) + V \sum_{\langle i,j \rangle} \hat{n}_i \hat{n}_j. \quad (2)$$

$t_1$  and  $t_2$  are the NN and next-nearest-neighbor (NNN) hopping constants, respectively. Same as before,  $V$  represents the NN interaction strength. A phase  $\phi_{ij} = \frac{\pi}{2}$  ( $-\frac{\pi}{2}$ ) in the anticlockwise (clockwise) loops is added to the second hopping term, which breaks the time-reversal symmetry and turns the system to be topologically non-trivial.

To explain the intensity of the high-harmonic spectroscopy in correlated systems, we calculate the real part of the optical conductivity in equilibrium, which is given by the Kubo formula:

$$\text{Re } \sigma(\omega) = \frac{\pi}{L} \sum_{m \neq 0} |\langle \psi_m | \hat{j} | \psi_0 \rangle|^2 \delta(\omega + E_m - E_0) \quad (3)$$

where  $|\psi_0\rangle$  and  $|\psi_m\rangle$  are the ground state and  $m$ -th eigenstate, respectively. Eq. (3) only gives the the optical conductivity with finite frequency because  $m \neq 0$ . The delta function is broadened by using a Lorentzian shape with a broadening factor  $\eta = 0.1$ . The current operator  $\hat{j} = -it_1 \sum_{\langle i,j \rangle, \sigma} [\hat{c}_{i,\sigma}^\dagger \hat{c}_{j,\sigma} - \text{H.c.}]$  on the 1D chain, while on the 2D honeycomb lattice we have

$$\hat{j}_x = -it_1 \sum_{\langle i,j \rangle, \sigma} \mathbf{R}_{ij} \cdot \mathbf{e}_x [\hat{c}_{i,\sigma}^\dagger \hat{c}_{j,\sigma} - \text{H.c.}] - it_2 \sum_{\langle\langle i,j \rangle\rangle, \sigma} \mathbf{R}_{ij} \cdot \mathbf{e}_x [e^{i\phi_{ij}} \hat{c}_{i,\sigma}^\dagger \hat{c}_{j,\sigma} - \text{H.c.}], \quad (4)$$

where  $\mathbf{R}_{ij} = \mathbf{R}_j - \mathbf{R}_i$  and the  $x$  direction is defined to be along the nearest-neighbour sites.

Out of equilibrium, we calculate the time-dependent current  $\langle j \rangle_t = \langle \psi(t) | \hat{j} | \psi(t) \rangle$  in 1D and  $\langle j_x \rangle_t = \langle \psi(t) | \hat{j}_x | \psi(t) \rangle$  in 2D. The HHG spectrum  $|\langle j \rangle_\omega|^2$  is obtained as the modulus square of the Fourier transform of the time-dependent current  $\langle j \rangle_t$  or  $\langle j_x \rangle_t$ . We adopt the

time-dependent Lanczos technique in ED to evolve the many-body wave function, see more details in Appendix A. The external electric field during photoirradiation can be included into the Hamiltonian via the Peierls substitution in the hopping terms:

$$\hat{c}_{i,\sigma}^\dagger \hat{c}_{j,\sigma} + \text{H.c.} \rightarrow e^{i\mathbf{A}(t) \cdot (\mathbf{R}_j - \mathbf{R}_i)} \hat{c}_{i,\sigma}^\dagger \hat{c}_{j,\sigma} + \text{H.c.}, \quad (5)$$

where  $\mathbf{A}(t) = (A_x(t), A_y(t))$  is the vector potential and

$$A_x(t) = \begin{cases} A_{0,x} e^{-t^2/2t_d^2} \cos(\omega_0 t), & t < 0 \\ A_{0,x} \cos(\omega_0 t), & t \geq 0 \end{cases} \quad (6)$$

$$A_y(t) = \begin{cases} A_{0,y} e^{-t^2/2t_d^2} \sin(\omega_0 t), & t < 0 \\ A_{0,y} \sin(\omega_0 t), & t \geq 0. \end{cases} \quad (7)$$

The parameter  $t_d$  controls the width of the Gaussian-like envelope with  $t < 0$  and  $\omega_0$  is the fundamental frequency of incident light. In the 2D case, we set  $A_{0,x} = A_{0,y}$  to simulate the circularly polarized laser, while in the case of 1D chain, we set  $A_{0,y} = 0$  to simulate the linearly polarized one. For convenience, we just use  $A_0$  instead of  $A_{0,x}$  to denote the amplitude of the laser in the 1D case.

In the rest of this letter, we use the unit with  $e = \hbar = c = 1$ , and the lattice spacing  $a_0 = 1$ . In this unit,  $t_1$  and  $t_1^{-1}$  are set to be the unit of energy and time, respectively.

*Results.*— We first study the extended Hubbard model on the periodic chain, whose phase diagram is detailed in Ref. [41]. We set  $U = 10.0$  and the phase transition between SDW and CDW locates at  $V \simeq U/2 = 5.0$ . Figure 1 (a) shows the optical conductivity  $\text{Re } \sigma(\omega)$  in equilibrium with changing the NN interaction  $V$ , where we can observe a minimum optical gap at  $V = 5.0$ . Such features have also been studied in Ref. [42], together with a minimum of the single-particle gap.

The HHG spectrum  $|\langle j \rangle_\omega|^2$  as a function of  $\omega/\omega_0$  and the interaction  $V$  are plotted in Figs. 1 (b) and (c), with  $\omega_0 = 0.1$ ,  $A_0 = 10.0$  and  $\omega_0 = 0.2$ ,  $A_0 = 5.0$ , respectively. Interestingly, there is an obvious enhancement of HHG spectrum approaching to the critical point  $V = 5.0$ . This can serve as an optical tool to detect the QCP between two insulating phases, which can not be directly measured by the traditional electrical methods. In SDW and CDW phases, the harmonic orders with high intensity of HHG have a very good correspondence with the optical conductivity through multiplied by the fundamental frequency  $\omega_0$ . Difference is that in CDW regime, the HHG spectrum loses its weight gradually with the increasing of  $V$ . From the definition of Eq. (3), we know that the spectra of optical conductivity are associated with the corresponding excited states that can be connected to the ground state by the current operator. These excited states are called the optically allowed states. The HHG is a kind of nonlinear process with absorbing  $m$  multiples of

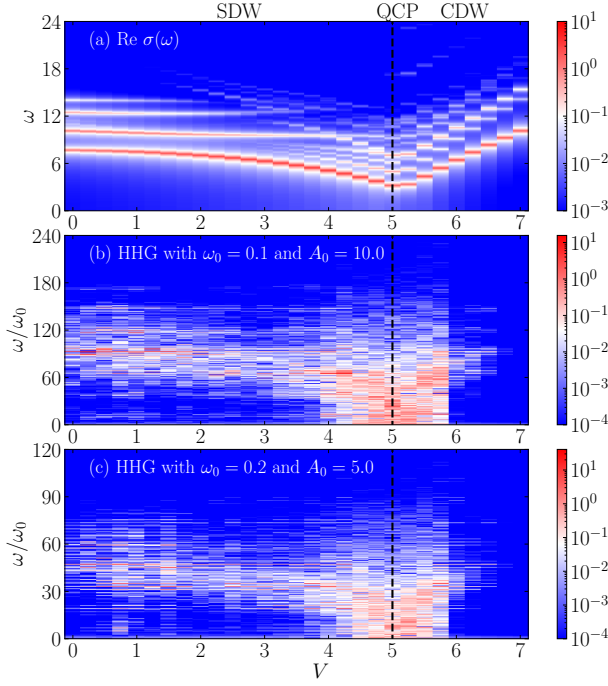


FIG. 1. (a) Contour plots of the optical conductivity  $\text{Re } \sigma(\omega)$  as a function of  $\omega$  and the NN interactions  $V$ . Contour plots of HHG spectrum  $|\langle j \rangle_\omega|^2$  as a function of  $\omega/\omega_0$  and  $V$ , with  $\omega_0 = 0.1$  and  $A_0 = 10.0$  in (b) as well as  $\omega_0 = 0.2$  and  $A_0 = 5.0$  in (c). Other parameters of the Hamiltonian (1) and the external laser are set to be  $U = 10.0$  and  $t_d = 50.0$ .

photons and generating laser with frequency  $m$  multiples of the incident light. Thus, the integer  $m$  strongly depends on the energy difference between the ground state and the optically allowed states, which explains the similarity between the optical conductivity and HHG spectrum. This feature may provide a new way to predict the HHG plateau and cut-off energy in correlated materials. For the case of  $V = 5.0$ , there are more optically allowed states in the vicinity of the critical point, as shown in Fig. 1 (a). We speculate that electron hoppings between these optically allowed excited states contribute to more harmonic generation with lower frequency. We propose that such an intriguing phenomenon could be utilized to generate HHG with higher strength. In addition, the fact that intensity of HHG in CDW phase with larger  $V$  becomes more and more weak can be attributed to the rapid increment of the optical gap, i.e., the energy difference between the ground state and the lowest optical allowed excited state.

Now we start to discuss the details of the HHG spectrum and the ultrafast dynamics of 1D extended Hubbard model. We choose  $V = 0$  and  $V = 6$  in SDW and CDW phase, respectively, and  $V = 5$  very close to the critical point to plot  $|\langle j \rangle_\omega|^2$  as a function of  $\omega/\omega_0$ , see Figs. 2 (a), (b) and (c). In order to obtain  $|\langle j \rangle_\omega|^2$ , we do the Fourier transform of  $\langle j \rangle_t$  from  $t = -300$  to  $t = 400$ . In

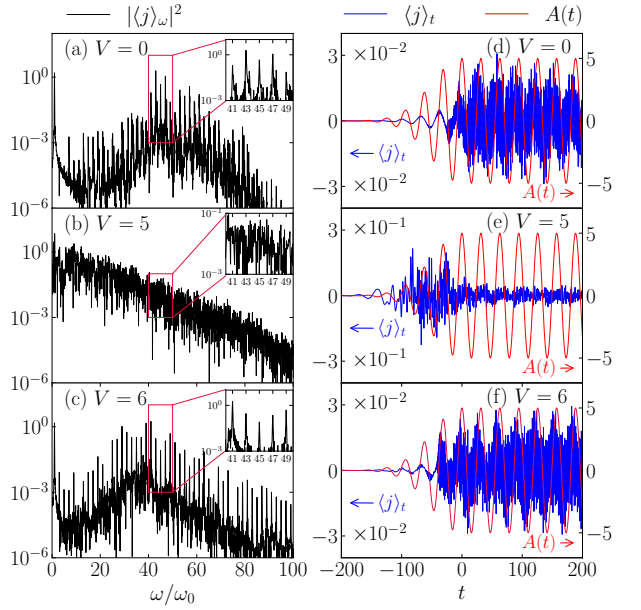


FIG. 2. The HHG spectrum  $|\langle j \rangle_\omega|^2$  as a function of  $\omega/\omega_0$  with  $V = 0.0$  (a),  $V = 5.0$  (b) and  $V = 6.0$  (c). Time profiles of  $A(t)$  (red lines) and  $\langle j \rangle_t$  (blue lines) with  $V = 0.0$  (d),  $V = 5.0$  (e) and  $V = 6.0$  (f). Other parameters of the Hamiltonian (1) and the external laser are set to be  $U = 10.0$ ,  $\omega_0 = 0.2$ ,  $A_0 = 5.0$  and  $t_d = 50.0$ .

SDW and CDW phases, all the sharp peaks of HHG spectrum locates at  $\omega/\omega_0 = 2n + 1$  with  $n > 0$ , i.e., the odd number of harmonic order. However, one can not clearly distinguish the harmonic components of the HHG with  $V = 5.0$ . This is due to the rapid thermalization near the critical point, which has also been studied in Ref. [43] that the electronic thermalization becomes stronger with the increasing of  $V$  in SDW phase. To examine this idea, we plot the time evolution of the current  $\langle j \rangle_t$  (blue lines) and time profiles of the vector potential  $A(t)$  (red lines) in Figs. 2 (d), (e) and (f). We can find a quick and intense current response in the case of  $V = 5.0$  with the order of magnitude being  $10^{-1}$  when the light starts to pump in. As the light shining steadily ( $t > 0$ ), an obvious suppression of the current response takes place and the irregular oscillation appears. The reason is that the extra energy injected from the light to the electronic systems leads to a dramatic thermalization because of the absence of extra degrees of freedoms in our model such as the phonon bath. The reference [44] also reported that the peaks of their odd-order harmonics get cleaner by introducing the imaginary potential to phenomenologically depict the dephasing process in the solid HHG. While in our case, there is no such channels to dissipate the injected energy, which cause the consequent thermalization. In addition, current responses of  $\langle j \rangle_t$  inside SDW and CDW phase seem to be regular with one order of magnitude smaller than the case of  $V = 5..$

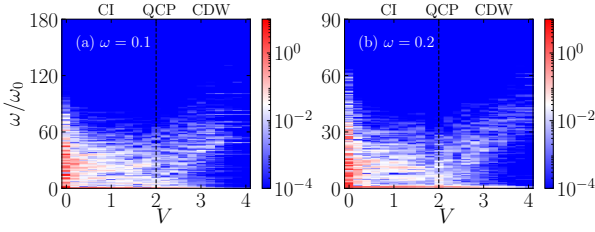


FIG. 3. Contour plots of HHG spectrum  $|\langle j \rangle_\omega|^2$  as a function of  $\omega/\omega_0$  and  $V$ , with  $\omega_0 = 0.1$  in (a) and  $\omega_0 = 0.2$  in (b). Other parameters of the Hamiltonian (2) and the external laser are set to be  $t_2 = 0.2$ ,  $A_{0,x} = 10.0$ ,  $A_{0,y} = 10.0$  and  $t_d = 50.0$ .

For the interacting spinless Haldane model (2), the topological phase transition from a Chern insulator (CI) towards a trivial CDW insulator with growing interactions has been studied by Varney et al [45, 46]. Here we adopt the 24A lattice with periodic boundary condition shown in the inset of Fig. 4 (b), which can largely reduce the finite-size effect because of its good symmetry [46]. We set  $t_2 = 0.2$  and the QCP locates at  $V \approx 2.0$ . Contour plots of the HHG spectrum  $|\langle j \rangle_\omega|^2$  as a function of  $\omega/\omega_0$  and  $V$  are shown in Figs. 3 (a) and (b), with the incident laser frequency  $\omega_0 = 0.1$  and  $\omega_0 = 0.2$ , respectively. Other parameters of the external circularly polarized laser are set to be  $A_{0,x} = 10.0$ ,  $A_{0,y} = 10.0$  and  $t_d = 50.0$ . Instead of enhancement of HHG close to QCP, we observe a gradually decreasing of the HHG intensity with  $V$  increasing. So we speculate this is due to the gapless CI phase and there are already enough low-energy excited states to contribute the harmonic generation in the topological phase. This supports that the topological edge states inside the bulk gap might favor a stronger HHG.

To see more details of the electron dynamics, we show the time-evolution of  $\langle j_x \rangle_t$  for different  $V$  in the right panel of Fig. 4. With  $V$  increasing from 0 to 4, amplitudes of the current responses decrease from the order of  $10^{-1}$  to  $10^{-3}$ , as shown in Figs. 4 (d), (e) and (f). This results in a weaker HHG intensity for larger  $V$ , as seen in Figs. 4 (a), (b) and (c). Similar to the 1D case, there is a apparent thermalization occurring soon after applying the light to system with  $V = 2.0$ . However, the thermalization in the 2D case comes more rapidly and completely. By inspecting Figs. 4 (a) and (c) as well as their subplots carefully, we find that there are both odd- and even-order components of HHG when  $V = 0$  in the CI phase, while most harmonic order in CDW side are odd numbers with a suppression of the peaks for the number  $3 \times (2n + 1)$ . Such  $3 \times (2n + 1)$  peaks could be observed by adopting another shape of 24-site lattice (see Appendix C for details), but the even-order number peaks can not be revisited by changing shape or lattice size. So we propose that the odd- or even-order com-

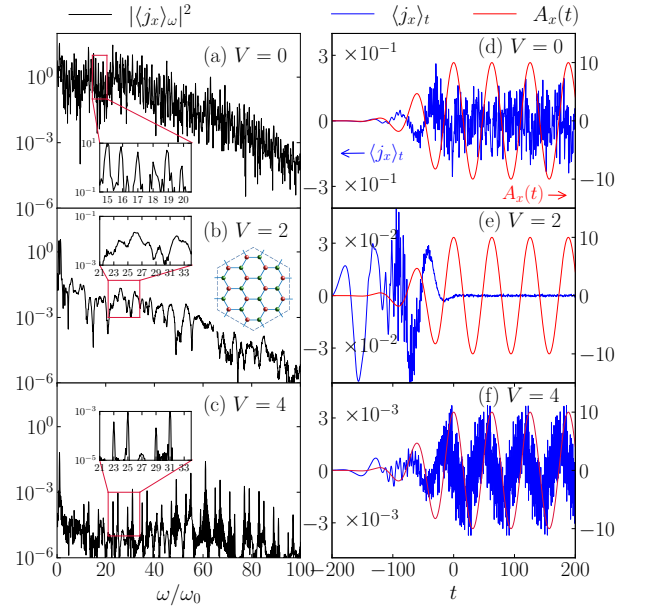


FIG. 4. The HHG spectrum  $|\langle j \rangle_\omega|^2$  as a function of  $\omega/\omega_0$  with  $V = 0.0$  (a),  $V = 2.0$  (b) and  $V = 4.0$  (c). Time profiles of  $A_x(t)$  (red lines) and  $\langle j_x \rangle_t$  (blue lines) with  $V = 0.0$  (d),  $V = 2.0$  (e) and  $V = 4.0$  (f). Other parameters of the Hamiltonian (2) and the external laser are set to be  $t_2 = 0.2$ ,  $\omega_0 = 0.1$ ,  $A_0 = 10.0$  and  $t_d = 50.0$ .

ponents of HHG spectrum can be utilized to distinguish topologically and locally ordered states.

*Summary and discussion.*— Quantum phase transition and its critical behavior are playing an important role in the field of condensed matter physics. By studying the extended Hubbard model on the periodic chain, we found that the optical-allowed excited states, which can be measured by optical conductivity in equilibrium, contribute the formation of HHG spectrum. When the system is close to the critical point which separates two gapped phases, more intense HHG especially in low frequencies is observed because there are more optical allowed excited states. Such phenomenon can be reproduced in the same model on a two-leg ladder, see Appendix B for more details. For the interacting Haldane model on the honeycom lattice, enhancement of HHG close to the topological phase transition point is not observed because the original CI phase is gapless. However, the odd- or even-order components of HHG spectrum provide another way to detect the QPT.

The issue remains open about whether the enhancement of HHG intensity can be accessed in ultrafast experiments for some materials. The candidates include the quasi-1D organic Mott insulators of the TCNQ family [47], in particular ET-F<sub>2</sub>TCNQ which is widely studied because of the existence of both on-site and NN Coulomb repulsions ( $t_1 \sim 0.1\text{eV}$ ,  $U \sim 1\text{eV}$ ; refs.[48, 49]). In addition, the search can be extended to ladder or 2D



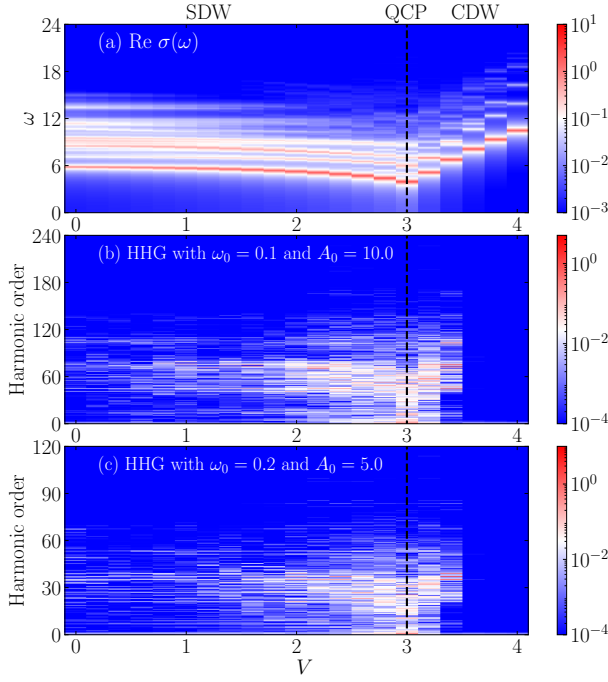


FIG. 5. (a) Contour plots of the optical conductivity  $\text{Re } \sigma(\omega)$  as a function of  $\omega$  and the NN interactions  $V$ . Contour plots of HHG spectrum  $|\langle j \rangle_\omega|^2$  as a function of  $\omega/\omega_0$  and  $V$ , with  $\omega_0 = 0.1$  and  $A_0 = 10.0$  in (b) as well as  $\omega_0 = 0.2$  and  $A_0 = 5.0$  in (c). Other parameters of the two-leg extended Hubbard model and the external laser are set to be  $U = 9.0$  and  $t_d = 50.0$ .

materials at half-filling with strong electron correlations, such as  $\text{Sr}_{14-x}\text{Ca}_x\text{Cu}_{24}\text{O}_{41}$  [50, 51].

### Appendix A: Time-dependent Lanczos method

For the time-dependent Hamiltonian  $\hat{H}(t)$ , we apply the time-dependent Lanczos method to evolve the time-dependent wave function  $|\psi(t)\rangle$  starting from the initial ground state [52], via

$$|\psi(t + \delta t)\rangle \simeq \sum_{l=1}^M e^{-i\epsilon_l \delta t} |\phi_l\rangle \langle \phi_l | \psi(t)\rangle, \quad (8)$$

where  $\epsilon_l$  and  $|\phi_l\rangle$  are eigenvalues and eigenvectors of  $\hat{H}(t)$ , respectively, in the Krylov subspace;  $M$  is the dimension of the Lanczos basis, and  $\delta t$  is the time stepping. We select  $M = 30$  and  $\delta t = 0.02$  to ensure the convergence of numerical evolution within  $t \leq 700$ . The validity of this method has also been checked by lots of references, such as Ref. 53.

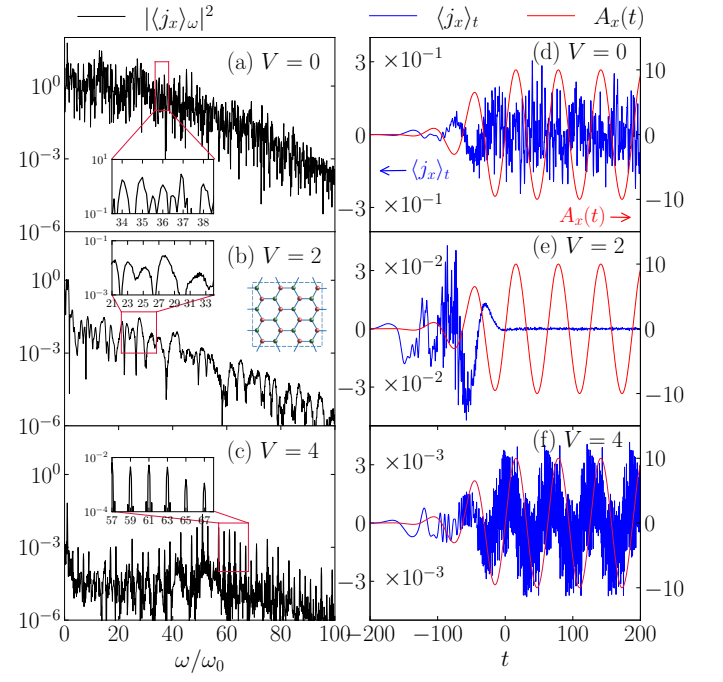


FIG. 6. The HHG spectrum  $|\langle j \rangle_\omega|^2$  as a function of  $\omega/\omega_0$  with  $V = 0.0$  (a),  $V = 2.0$  (b) and  $V = 4.0$  (c). Time profiles of  $A_x(t)$  (red lines) and  $\langle j_x \rangle_t$  (blue lines) with  $V = 0.0$  (d),  $V = 2.0$  (e) and  $V = 4.0$  (f). Other parameters of the interacting Haldane model and the external laser are set to be  $t_2 = 0.2$ ,  $\omega_0 = 0.1$ ,  $A_0 = 10.0$  and  $t_d = 50.0$ .

### Appendix B: HHG spectrum of the extended Hubbard model on a two-leg ladder.

In this part, we choose a two-leg ladder with the lattice size  $L = 2 \times 6 = 12$  to calculate the HHG spectrum of the extended Hubbard model. The periodic and open boundary conditions are applied along the leg and rung, respectively. The external laser to generate HHG is set to be linearly polarized along the leg and the optical conductivity  $\text{Re } \sigma(\omega)$  is also defined along this direction. The on-site interaction  $U = 9$  and phase diagram between the spin-density-wave (SDW) and charge-density-wave (CDW) states locates at  $V \approx U/3 = 3.0$  [54]. We plot  $\text{Re } \sigma(\omega)$  in equilibrium with changing the nearest-neighbour (NN) interaction  $V$  in Fig. 5 (a), which shows a minimum optical gap at  $V = 3.0$ .

The parameters of the external laser are same with those in 1D chain in the main text:  $\omega_0 = 0.1$  and  $A_0 = 10.0$  in Fig. 5 (b);  $\omega_0 = 0.2$  and  $A_0 = 5.0$  in Fig. 5 (c).  $t_d = 50.0$  for the both figures. We could also observe an enhancement of the HHG intensity when the system is approaching the critical point. We believe this feature should be observed if the critical point separating two gapped phases because of the high sensitivity of system.

### Appendix C: HHG spectrum of the Interacting Haldane model on the 24C honeycomb lattice

In the main text, we show that on the 24A honeycomb lattice, odd-order HHG with a suppression of the peaks with number  $3(2n+1)$  is manifested in CDW phase of the Haldane model with NN interactions. In this section, to check the finite-size effect, a 24C lattice shown in Fig. 6 (b) is adopted. We do the same calculation with Fig. 4 in the main text. Similarly, we can find that both odd- and even-order harmonic generations can be observed in the Chern insulator with  $V = 0$ , see in Fig. 6 (a) and its inset. The rapid and complete thermalization also occurs when the system is close to the critical point  $V = 2$  [see Fig. 6 (e)], which leads to a weak and unclear order of HHG shown in Fig. 6 (b). In CDW phase, we find that most odd-order HHG peaks can be observed, which is different from the fact that the peaks with number  $3(2n+1)$  are suppressed in 24A lattice. The results further support our proposal to use the odd- or even-order components to distinguish topological and local-order phases.

---

\* shaocan@njust.edu.cn

† rfu@njust.edu.cn

- [1] S. Sachdev, *Quantum Phase Transitions*, 2nd ed. (Cambridge University Press, Cambridge, United Kingdom, 2011).
- [2] M. Vojta, *Reports on Progress in Physics* **66**, 2069 (2003).
- [3] N. D. Mathur, F. M. Grosche, S. R. Julian, I. R. Walker, D. M. Freye, R. K. W. Haselwimmer, and G. G. Lonzarich, *Nature* **394**, 39 (1998).
- [4] A. Osterloh, L. Amico, G. Falci, and R. Fazio, *Nature* **416**, 608 (2002).
- [5] X. Peng, J. Du, and D. Suter, *Phys. Rev. A* **71**, 012307 (2005).
- [6] J. Zhang, X. Peng, N. Rajendran, and D. Suter, *Phys. Rev. Lett.* **100**, 100501 (2008).
- [7] A. Lucas, S. Gazit, D. Podolsky, and W. Witczak-Krempa, *Phys. Rev. Lett.* **118**, 056601 (2017).
- [8] M.-C. Cha, M. P. A. Fisher, S. M. Girvin, M. Wallin, and A. P. Young, *Phys. Rev. B* **44**, 6883 (1991).
- [9] K. Damle and S. Sachdev, *Phys. Rev. B* **56**, 8714 (1997).
- [10] J. Šmakov and E. Sørensen, *Phys. Rev. Lett.* **95**, 180603 (2005).
- [11] W. Witczak-Krempa, P. Ghaemi, T. Senthil, and Y. B. Kim, *Phys. Rev. B* **86**, 245102 (2012).
- [12] R. C. Myers, S. Sachdev, and A. Singh, *Phys. Rev. D* **83**, 066017 (2011).
- [13] W. Witczak-Krempa and S. Sachdev, *Phys. Rev. B* **86**, 235115 (2012).
- [14] W. Witczak-Krempa, E. S. Sørensen, and S. Sachdev, *Nature Physics* **10**, 361 (2014).
- [15] K. Chen, L. Liu, Y. Deng, L. Pollet, and N. Prokof'ev, *Phys. Rev. Lett.* **112**, 030402 (2014).
- [16] S. Gazit, D. Podolsky, A. Auerbach, and D. P. Arovas, *Phys. Rev. B* **88**, 235108 (2013).
- [17] E. Katz, S. Sachdev, E. S. Sørensen, and W. Witczak-Krempa, *Phys. Rev. B* **90**, 245109 (2014).
- [18] S. Gazit, D. Podolsky, and A. Auerbach, *Phys. Rev. Lett.* **113**, 240601 (2014).
- [19] W. Witczak-Krempa and J. Maciejko, *Phys. Rev. Lett.* **116**, 100402 (2016).
- [20] H. T. Quan, Z. Song, X. F. Liu, P. Zanardi, and C. P. Sun, *Phys. Rev. Lett.* **96**, 140604 (2006).
- [21] Z.-G. Yuan, P. Zhang, and S.-S. Li, *Phys. Rev. A* **75**, 012102 (2007).
- [22] T. Brabec and F. Krausz, *Rev. Mod. Phys.* **72**, 545 (2000).
- [23] P. B. Corkum and F. Krausz, *Nature Physics* **3**, 381 (2007).
- [24] A. L. Cavalieri, N. Müller, T. Uphues, V. S. Yakovlev, A. Baltuška, B. Horvath, B. Schmidt, L. Blümel, R. Holzwarth, S. Hendel, M. Drescher, U. Kleineberg, P. M. Echenique, R. Kienberger, F. Krausz, and U. Heinzmann, *Nature* **449**, 1029 (2007).
- [25] F. Krausz and M. Ivanov, *Rev. Mod. Phys.* **81**, 163 (2009).
- [26] P. Agostini and L. F. DiMauro, *Reports on Progress in Physics* **67**, 813 (2004).
- [27] L. Gallmann, C. Cirelli, and U. Keller, *Annual Review of Physical Chemistry* **63**, 447 (2012).
- [28] P. B. Corkum, *Phys. Rev. Lett.* **71**, 1994 (1993).
- [29] M. Lewenstein, P. Balcou, M. Y. Ivanov, A. L'Huillier, and P. B. Corkum, *Phys. Rev. A* **49**, 2117 (1994).
- [30] K. L. Ishikawa and T. Sato, *IEEE Journal of Selected Topics in Quantum Electronics* **21**, 1 (2015).
- [31] S. Ghimire, A. D. DiChiara, E. Sistrunk, P. Agostini, L. F. DiMauro, and D. A. Reis, *Nature Physics* **7**, 138 (2011).
- [32] G. Vampa, C. R. McDonald, G. Orlando, D. D. Klug, P. B. Corkum, and T. Brabec, *Phys. Rev. Lett.* **113**, 073901 (2014).
- [33] S. Y. Kruchinin, F. Krausz, and V. S. Yakovlev, *Rev. Mod. Phys.* **90**, 021002 (2018).
- [34] U. Huttner, M. Kira, and S. W. Koch, *Laser & Photonics Reviews* **11**, 1700049 (2017).
- [35] S. Ghimire and D. A. Reis, *Nature Physics* **15**, 10 (2019).
- [36] C. Yu, S. Jiang, and R. Lu, *Advances in Physics: X* **4**, 1562982 (2019).
- [37] Y. Murakami, M. Eckstein, and P. Werner, *Phys. Rev. Lett.* **121**, 057405 (2018).
- [38] S. Imai, A. Ono, and S. Ishihara, *Phys. Rev. Lett.* **124**, 157404 (2020).
- [39] S. de Vega, J. D. Cox, F. Sols, and F. J. García de Abajo, *Phys. Rev. Research* **2**, 013313 (2020).
- [40] R. E. F. Silva, I. V. Blinov, A. N. Rubtsov, O. Smirnova, and M. Ivanov, *Nature Photonics* **12**, 266 (2018).
- [41] S. Ejima and S. Nishimoto, *Phys. Rev. Lett.* **99**, 216403 (2007).
- [42] C. Shao, T. Tohyama, H.-G. Luo, and H. Lu, *Phys. Rev. B* **101**, 045128 (2020).
- [43] C. Shao, T. Tohyama, H.-G. Luo, and H. Lu, *Phys. Rev. B* **99**, 035121 (2019).
- [44] G. Wang and T.-Y. Du, *Phys. Rev. A* **103**, 063109 (2021).
- [45] C. N. Varney, K. Sun, M. Rigol, and V. Galitski, *Phys. Rev. B* **82**, 115125 (2010).
- [46] C. N. Varney, K. Sun, M. Rigol, and V. Galitski, *Phys. Rev. B* **84**, 241105 (2011).
- [47] H. Uemura, H. Matsuzaki, Y. Takahashi, T. Hasegawa, and H. Okamoto, *Journal of the Physical Society of Japan*

- [77](#), [113714](#) (2008).
- [48] S. Wall, D. Brida, S. R. Clark, H. P. Ehrke, D. Jaksch, A. Ardavan, S. Bonora, H. Uemura, Y. Takahashi, T. Hasegawa, H. Okamoto, G. Cerullo, and A. Cavalleri, [Nature Physics](#) **7**, [114](#) (2011).
  - [49] T. Hasegawa, T. Mochida, R. Kondo, S. Kagoshima, Y. Iwasa, T. Akutagawa, T. Nakamura, and G. Saito, [Phys. Rev. B](#) **62**, [10059](#) (2000).
  - [50] R. Fukaya, Y. Okimoto, M. Kunitomo, K. Onda, T. Ishikawa, S. Koshihara, H. Hashimoto, S. Ishihara, A. Isayama, H. Yui, and T. Sasagawa, [Nature Communications](#) **6**, [8519](#) (2015).
  - [51] T. Osafune, N. Motoyama, H. Eisaki, and S. Uchida, [Phys. Rev. Lett.](#) **78**, [1980](#) (1997).
  - [52] P. Prelovšek and J. Bonča, in *Strongly Correlated Systems-Numerical Methods*, edited by A. Avella and F. Mancini, Springer Series in Solid-State Sciences, Vol. 176 (Springer, Berlin, 2013), pp. 1-30.
  - [53] C. Shao, T. Tohyama, H.-G. Luo, and H. Lu, [Phys. Rev. B](#) **93**, [195144](#) (2016).
  - [54] M. Vojta, R. E. Hetzel, and R. M. Noack, [Phys. Rev. B](#) **60**, [R8417](#) (1999).